Analysis of Large Vortical Structures in Shear Layers

Roy M. McInville*
North Carolina State University, Raleigh, North Carolina
T. B. Gatski†
NASA Langley Research Center, Hampton, Virginia
and
H. A. Hassan‡
North Carolina State University, Raleigh, North Carolina

One of the most promising methods of minimizing drag is the reduction of skin friction by the injection of low-momentum fluid into the near-wall region of turbulent boundary-layer flows. This method could be made more effective by limiting the spread rate of the resulting mixing region. In order to achieve a better understanding of how this goal might be achieved, numerical investigations of the relevant fluid dynamic processes governing these regions have been conducted. A compact finite difference algorithm has been applied to the complete form of the governing conservation equations for a two-dimensional laminar mixing layer. The ability of this computational approach to model successfully the formation and interaction of the large-scale vortical structures dominating such flowfields is verified in the present study. Parameters affecting the spread rate of the mixing region are also identified and found to be consistent with experimental studies. In addition, the relative importance of viscous and momentum transport effects in the vortex interactions is determined.

Introduction

THE continuing escalation of energy costs in recent years has made the efficient use of available fuel resources a subject of major concern. For air transport systems, this implies reducing the overall vehicle drag to a minimum. Skin friction, which can account for up to 50% of the total drag on long-range transports and general aviation jets, has been identified as the area where greatest improvements might be realized.[1] One technique for achieving significant skin-friction reductions is the injection of low-momentum fluid through a slot into the near-wall region of the boundary layer.[2,3] Figure 1 shows a typical arrangement. The lower-velocity fluid produces a region of decreased surface drag. At the interface of the two streams, a mixing layer develops and begins to spread as it moves downstream. Once this region reaches the wall, viscous drag levels return monotonically to near-freestream values. Thus, if the shear layer spread rate could be slowed, greater drag reductions would be realized.

Experimental studies[4-8] have shown that such mixing regions are characterized by the presence of large-scale vortical structures formed by the roll-up of the developing shear layer. The growth and interaction of these entities determines, to a large extent, the spatial and temporal evolution of the flowfield. Specifically, the coalescence of two or more of these relatively discrete vortices into a single larger structure has been found to be the primary source of mixing growth.[6-8] Thus, an understanding of the physics governing this process is essential to the manipulation of the spread rate.

Received Dec. 21, 1983; presented as Paper 84-0349 at the AIAA 22nd Aerospace Sciences Meeting, Reno, NV, Jan. 9-12, 1984; revision received Nov. 12, 1984.

*Research Assistant, Mechanical and Aerospace Engineering Department. Student Member AIAA.
†Research Scientist, Viscous Flow Branch, High Speed Aerodynamics Division.
‡Professor, Mechanical and Aerospace Engineering Department. Associate Fellow AIAA.

The present work addresses this problem by applying a compact finite difference scheme[9,10] to the complete form of the governing conservation equations for a two-dimensional mixing layer. It should be emphasized that, since a laminar code is used, the effects of small-scale random turbulence are not included. However, the flowfields under consideration are dominated by large-scale velocity fluctuations associated with the coherent structures. Since these effects are accurately modeled, good computational results can be obtained.

This approach offers a distinct advantage over point vortex methods[11-14] since the generality of the equations permits detailed study of the relevant dynamic processes. In addition, this formulation of the problem permits observation of the downstream evolution of the vortical structures in their proper spatial and temporal relationships. This is in contrast to temporal mixing layer studies (e.g., Ref. 15) where nonparallel growth of the mixing layer is not allowed.

The validity of this approach has been verified by its application to several forced shear layers investigated experimentally in Ref. 8. In addition, information relating to the viscous and momentum transport terms has been extracted from the calculated velocity fields. An investigation of phase effects has shown the necessity of using a spatially accurate numerical scheme.

Approach

The governing conservation equations are formulated in velocity-vorticity variables as follows:

$$u_x + v_y = 0 \tag{1}$$

$$v_x - u_y = \zeta \tag{2}$$

$$\zeta_t + \mathrm{div}(V\zeta - \nu \mathrm{grad}\zeta) = 0 \tag{3}$$

where u and v are the x and y components, respectively, of the velocity vector V and ζ the vorticity. The streamwise coordinate is x and y the transverse coordinate. Subscripts denote differentiation.

The two-step solution procedure of Refs. 9 and 10 is used to advance the solution in time. First, given an initial vortic-

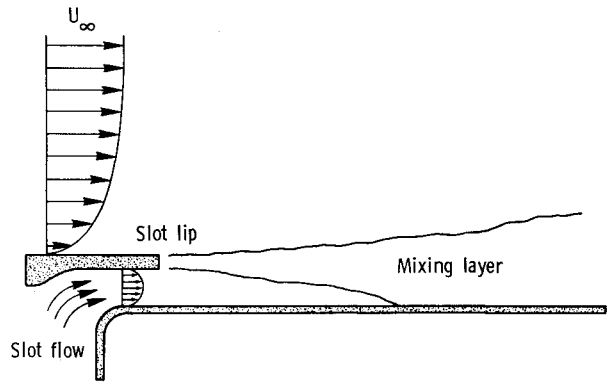

Fig. 1 Typical slot flow configuration.

ity field, the velocities are determined by applying Eqs. (1) and (2), together with appropriate averaging conditions, to each computational cell. A typical cell is shown in Fig. 2, with the dependent variables assigned to their respective locations on the cell. Values on cell edges are averages along that edge, while values of center cell variables are averages over the entire cell. In discretized form, the equations become

$$\delta_x u^n_{\cdot} + \delta_y v^n_{\cdot} = 0 \tag{4}$$

$$\delta_x v^n_{\cdot} - \delta_y u^n_{\cdot} = \zeta^{n-\frac{1}{2}} \tag{5}$$

$$(\mu_x - \mu_y) u^n_{\cdot} = 0 \tag{6}$$

$$(\mu_x - \mu_y) v^n_{\cdot} = 0 \tag{7}$$

where the periods denote spatial indices at the cell centers, n is the time index, and δ and μ are the standard difference and averaging operators defined below for a typical variable S and grid spacings Δx and Δy.

$$\delta_x S_{i,j} = (S_{i+\frac{1}{2},j} - S_{i-\frac{1}{2},j})/\Delta x_i \tag{8}$$

$$\delta_y S_{i,j} = (S_{i,j+\frac{1}{2}} - S_{i,j-\frac{1}{2}})/\Delta y_j \tag{9}$$

$$\mu_x S_{i,j} = (S_{i+\frac{1}{2},j} + S_{i-\frac{1}{2},j})/2 \tag{10}$$

$$\mu_y S_{i,j} = (S_{i,j+\frac{1}{2}} + S_{i,j-\frac{1}{2}})/2 \tag{11}$$

The resulting system of equations is solved by an SOR-type iteration scheme. Then, to obtain the new vorticity field, the vorticity transport equation is solved, together with averaging conditions, by an ADI-type scheme. In discretized form, these are

$$(\delta_t + (\mu_x u^n_{\cdot})\delta_x + (\mu_y v^n_{\cdot})\delta_y)\zeta^n_{\cdot} = \nu(\delta_x \phi^n_{\cdot} + \delta_y \psi^n_{\cdot}) \tag{12}$$

$$\mu_t \zeta^n_{\cdot} = \mu_x \zeta^n_{\cdot} = \mu_y \zeta^n_{\cdot} \tag{13}$$

where

$$\delta_x \zeta^n_{\cdot} = (\mu_x - \tfrac{1}{2}\Delta x_j q_x \delta_x)\phi^n_{\cdot} \tag{14}$$

$$\delta_y \zeta^n_{\cdot} = (\mu_y - \tfrac{1}{2}\Delta y_k q_y \delta_y)\psi^n_{\cdot} \tag{15}$$

and q_x, q_y are functions of the respective cell Reynolds numbers.[9,10] This completes one time step. For further details of the computational techniques, see Ref. 10.

At the top and bottom boundaries, $v=0$ conditions are imposed and held fixed for all time. The vorticities are calculated by second-order accurate differences at each time step. The downstream boundary is handled by applying outflow flux conditions on the v velocity and on the vorticity. This is done by moving the values at a distance $u\Delta t$ upstream out to the boundary for the next time step. To verify that this procedure produced satisfactory results, a case was run with the computational field extended 20% in the downstream direction. No changes in the vortex interaction processes were observed. At the inflow, values of u and the vorticity are specified. The velocity difference between the two streams is assumed to occur across a single computational cell on this boundary. The height of the cell is set equal to the initial maximum slope thickness of the shear layer, which is defined as

$$\text{Maximum slope thickness} = \frac{\Delta u}{(\partial u/\partial y)_{\max}} \tag{16}$$

The distribution of u values is assumed to be as shown in Fig. 3. The velocity difference between the two streams occurs at the center of the edge of the inflow computational cell located at $y=0.0$. This choice of location is made to fully utilize the fact that the variables defined at these edge locations are necessarily interpreted as average values across the edge.[9] To determine what value of u to assign to this cell, consider the following representation of the velocity field shown in Fig. 3:

$$U = U_2 H(y) + U_1[1 - H(y)] \tag{17}$$

where the Heaviside function is defined as,

$$\begin{aligned} H(y) &\equiv 0 \quad y<0 \\ &\equiv \tfrac{1}{2} \quad y=0 \\ &\equiv 1 \quad y>0 \end{aligned} \tag{18}$$

The required averaging of the functional form along the side of a cell gives an inflow u velocity value at $y=0.0$ of

$$\bar{U} = \tfrac{1}{2}(U_2 + U_1) \tag{19}$$

The manner of assigning vorticity boundary values at the inflow was found to be extremely critical. It is, of course, necessary to obtain vorticity values consistent with the velocity profile shown in Fig. 3 and represented by Eq. (17). Thus, vorticity values are zero at all inflow points, with the exception of the interface cell. At this cell the vorticity value is assumed to be given by

$$\zeta \simeq -\frac{\partial u}{\partial y} \tag{20}$$

Differentiating and then averaging the functional form of U [Eq. (17)] yields a value for ζ, at the interfacial cell, of

$$\zeta = -\frac{\partial U}{\partial y} = -\frac{U_2 - U_1}{\Delta y} \tag{21}$$

Forcing is provided by superimposing sinusoidal disturbances on the u values at the inflow boundary. Thus, we have

$$U_{\text{total}} = U + \sum_k a_k \sin(\omega_k t + \alpha_k) \tag{22}$$

where the a_k are disturbance amplitudes, ω_k their frequencies, and α_k their phase angles relative to the lowest frequency present and U is the unperturbed velocity at the inflow boundary.

Results

To validate the computational accuracy of the present approach, it was applied to the water tunnel investigations of

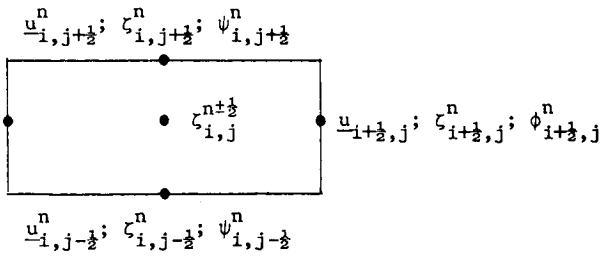

Fig. 2 Typical computational cell showing indexing of variables.

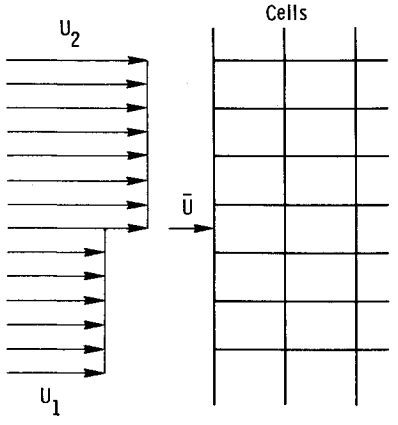

Fig. 3 Schematic of inflow boundary conditions.

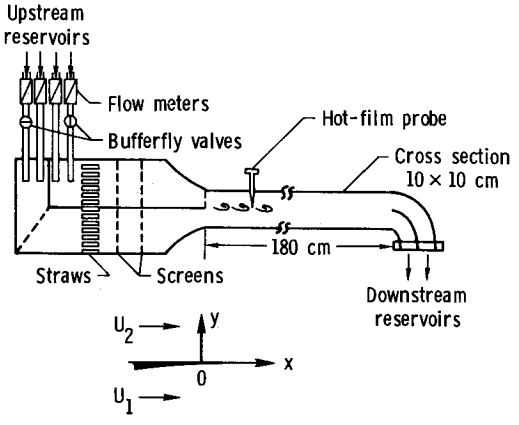

Fig. 4 Experimental apparatus.

Ref. 8. The experimental arrangement is shown in Fig. 4. Forcing was accomplished by introducing longitudinal velocity fluctuations into the flow by means of the butterfly values. Since the computational field begins at the shear layer origin, the amplitudes of these fluctuations measured at a point 16 mm downstream of the splitter plate were superimposed on the inflow u values.

Experimentally, with no forcing applied, only a periodic vortex formation was observed.[8] There was, however, a peak in the spectrum of the streamwise velocity fluctuations, which will be referred to as the most probable frequency f_m. This frequency was found to be about 5.06 Hz, which is close to the theoretical most amplified frequency.[8,15] It can be estimated for a given set of parameters as

$$St_m = f_m\theta/\bar{U} \approx 0.035 \tag{23}$$

where St_m is the corresponding Strouhal number, θ the momentum thickness, and $\bar{U}$ the mean velocity of the two streams.

Computationally, no vortex formation was observed in the unforced case. This apparent discrepancy is due to the presence of random background velocity fluctuations in the water tunnel of sufficient amplitude to trigger the irregular vortex formation that occurred. Unless specifically imposed, such background disturbances do not exist in the computational flowfield.

In the presence of forcing, several radically different mixing layer configurations were produced, depending on the frequencies used. The first of these, which shall be referred to as a mode I flow regime, is illustrated in Fig. 5. For this case, the forcing frequency is kept within the range of approximately 2.50-6.35 Hz. The lower limit corresponds roughly to the first subharmonic of f_m. The photograph of the water tunnel test section shows distinct periodic vortices, but no interactions between them. The response frequency, identified as the vortex passage frequency, matches the forcing. For the case shown, the forcing and the response frequencies are each equal to approximately 3.29 Hz. There is a definite streamwise elongation of each structure as it moves downstream, accompanied by diffusion. The vorticity contour map generated by the numerical scheme is shown in the same figure below the photograph. Of course, this type of comparison between the vorticity contours and the streaklines is qualitative, since only in the case of inviscid flow and time-independent inflow conditions would the lines of constant vorticity and streaklines coincide.[16] However, since the essential dynamics in the mixing layer flow is inviscid and the inflow unsteadiness is a relatively weak sinusoidal variation with zero time mean, it is not unreasonable to use the readily available vorticity values within the domain as a comparison basis. As Fig. 5 shows, the vorticity contours capture all of the relevant features of the mode I flowfield. Distinct vortices are clearly evident, but no interactions are indicated. Their passage frequency is equal to the forcing. The streamwise elongation is clearly shown and an inspection of the vorticity contours reveals its source. The structures are subjected to longitudinal shear stresses caused by the difference in velocity between the two streams of fluid. It can be clearly seen that the vortical fluid is swept downstream more quickly on the bottom, or high-speed, side than on the top. This results in the distortion of the vortex structures in the streamwise direction.

Figure 6 illustrates the mode II region that corresponds to forcing frequencies of approximately 1.60-2.50 Hz. This range extends roughly from the second to the first subharmonic of f_m. The top photograph shows the experimental flowfield.[8] The forcing frequency in this case is 1.62 Hz. Vortex formation occurs initially not at this frequency but at approximately 3.24 Hz, which is its first harmonic. Two vortices then merge to produce a downstream passage frequency of 1.62 Hz, which does correspond to the forcing. This pattern is typical of the mode II regime. The shear layer responds initially to a frequency close to f_m which, in this case, is the first harmonic of the forcing. The downstream amplification and subsequent saturation of the forcing frequency then causes the vortex pairing. The coalescence of the vortices is accompanied by a large increase in the spread rate of the mixing layer. This same behavior can be seen clearly in the numerically generated vorticity contour plot directly below the photograph.

A further decrease in forcing frequency below approximately 1.6 Hz produces a mode III configuration as shown in Fig. 7. The top photograph once again shows the test sec-

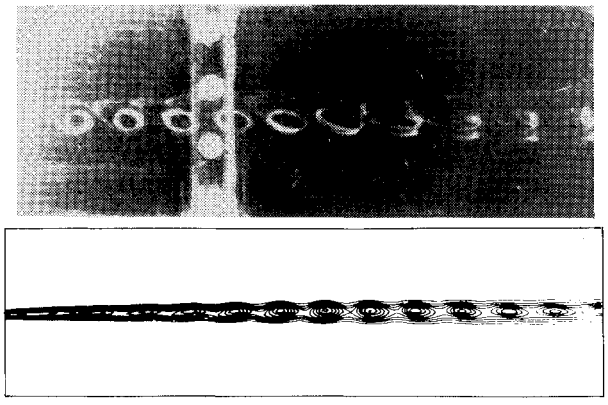

Fig. 5 Experimental flowfield and numerically generated vorticity contour plot for a mode I configuration.

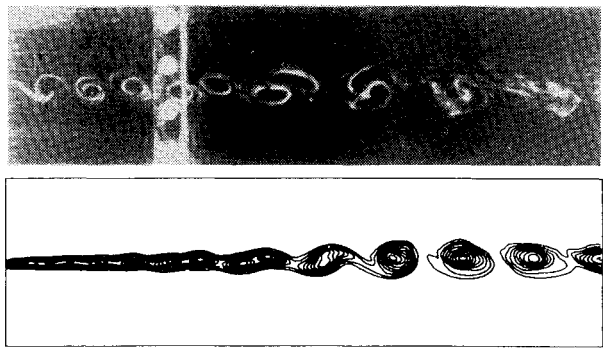

Fig. 6 Experimental flowfield and numerically generated vorticity contour plot for a mode II configuration.

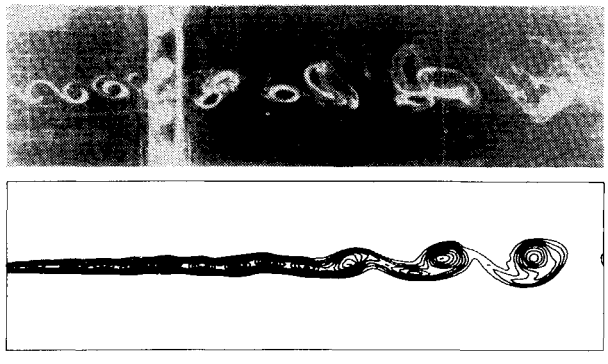

Fig. 7 Experimental flowfield and numerically generated vorticity contour plot for a mode III configuration.

tion flowfield.[8] The forcing frequency in this case is 1.06 Hz. The initial response now comes at approximately 3.18 Hz, corresponding to the second harmonic of the forcing. Once again, the sensitivity of the initial shear layer region to frequencies near f_m is indicated. In this flow regime, three vortices eventually merge under the influence of the forcing frequency that is amplified downstream. In most cases, two structures first coalesce and then this pair merges with the next trailing vortex. An increase in the spread accompanies this process. The vorticity contour map from the algorithm, located below the photograph, once again shows all of the relevant flowfield features.

Figure 8 shows a plot of the maximum slope thickness vs downstream distance for an unforced mixing layer. As can be seen, the calculated values agree quite well with those determined experimentally[8] up to about $x=13.0$ cm. It was at this point that random vortex pairings characterized by the linear growth rate of the region began to occur in the water tunnel. For the reasons mentioned earlier, this behavior is not exhibited by the numerical results.

Figure 9 gives the same information for a mode I mixing layer. Once again, the agreement is good up to the point where, in the experiment, random vortex pairings, triggered by the background velocity fluctuations, began to occur. Note that the calculations show a decrease in the shear layer width after it reaches a maximum. This effect is the result of momentum transfer mechanisms between the mean flow and the large-scale structures and will be discussed in detail later.

Figure 10 shows the spread rate of a mode II mixing layer. The divergence from experimental values at large x is once again apparent and expected. Otherwise, agreement is good except for a slight downstream shift in the calculated region of maximum growth relative to the corresponding region measured in the tunnel. This could be caused by the lack of resolution in the region near the left boundary where substantial amplification of the relevant frequencies occurs. This would result in a delay in the saturation point of the forcing frequency and thus move the vortex coalescence downstream. This shift accounts for the slightly higher calculated thickness after merging since a more developed mixing layer is present initially. It should be noted that the region of maximum spread is almost identical in spatial extent in both cases, covering a length of approximately four wavelengths of the initial response frequency. Also, in both cases, the mixing region almost exactly doubles in thickness during the coalescence process.

It is also possible to compare computed and experimental[8] mean velocity profiles for the mode II case. In order that the mean velocity profiles be compared correctly, it is necessary to use locations of equal momentum thicknesses as a basis of comparison. Figure 11 shows such a comparison at $x=14$ cm (see Fig. 23 of Ref. 8) and, as is seen, the agreement is quite good. This close quantitative and qualitative agreement between the developed velocity profiles indicates that the dominant mean flow features have been captured.

As a further verification of the numerical procedure, it is desirable to compare results from the fluctuating flowfield. Once again, the mode II case is studied. A comparison between the computed and experimental[8] rms streamwise fluctuating velocity component is shown in Fig. 12 at $x=12$ cm (see Fig. 29 of Ref. 8). The figure shows a fairly good quantitative and qualitative comparison between the results. Since this streamwise position is in a region of vortex merging, the nearly lateral alignment of two vortices is clearly represented by three distinct peaks in the figure. However, the lateral location of these computed peaks is slightly skewed relative to the experimental results[8] and the peak amplitudes are lower in the computed results. These discrepancies can be attributed to either insufficient numerical resolution in the vicinity of the peaks or to the absence of background turbulence that would augment the disturbance energetics, or both. It is apparent from the comparisons made between the computed and experimental[8] mean and fluctuating flowfields, that the numerical scheme has been able to model accurately the vortex interaction phenomenon. Later, additional insight into the merging process will be provided from an examination of the instantaneous and averaged fluctuating stresses present in the mixing layer.

In addition to the frequency of the applied perturbations, another factor that greatly affects the shear layer structure is the phase angle between the forcing and the initial response. Figure 13 demonstrates this for a mode II case. Here, the downstream propagation of vertical velocity perturbations, introduced at the left-hand boundary, is shown schematically. In Fig. 13a, the two frequencies are in phase. Initially, the shear layer is more sensitive to the response frequency and it will dominate, producing vertical displacements of fluid into either higher- or lower-velocity regions. Fluid displaced upward tends to be slowed and overtaken by that displaced downward into the higher velocity stream. This

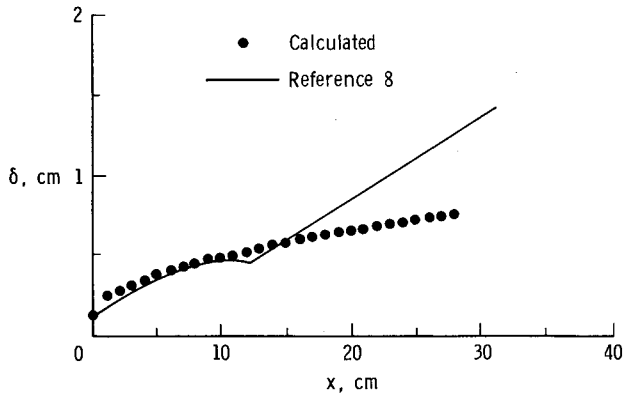

Fig. 8 Spread rate on an unforced mixing layer.

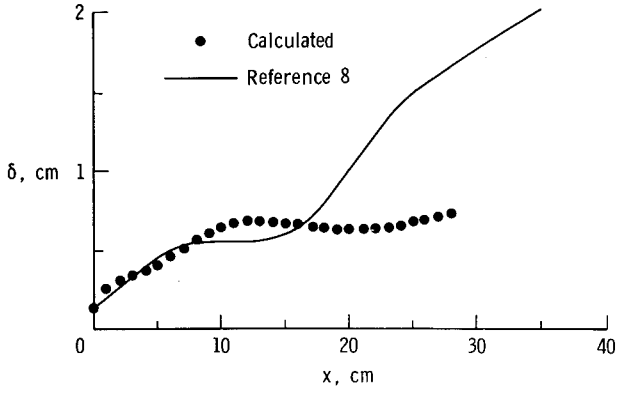

Fig. 9 Spread rate of mode I mixing layer.

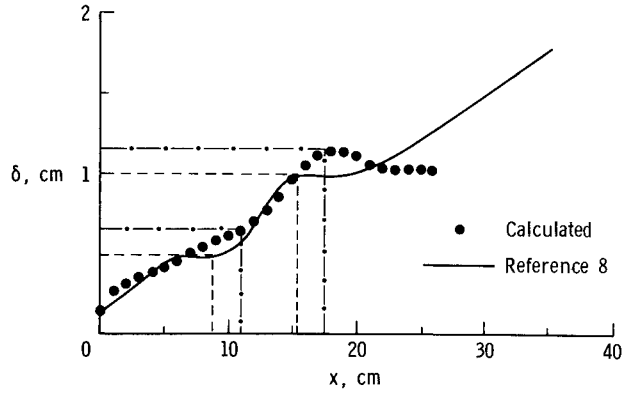

Fig. 10 Spread rate of a mode II mixing layer.

produces an initial vortex roll-up at the points marked by the asterisks. As can be seen, this places the vortices at the maxima of the forcing frequency curve. Thus, as it is amplified by the shear layer, maximum vertical displacement of the vortices is produced and those structures displaced into the high-speed flow will overtake those carried into the low-velocity side. The two vortices will then "roll" about each other and merge much like the regions of fluid that produced the initial shear layer roll-up.

Now, consider the case where the response and forcing perturbations are 180 deg out of phase. This situation is shown in Fig. 13b. The same reasoning applies as before, but now it can be seen that initial vortex formation will occur at the nodes of the forcing frequency curve. Thus, even with the downstream amplification of the forcing, no vertical displacements of the vortices will be produced and there will be no tendency for one to overtake another. Merging will be severely inhibited or absent altogether. Alternatively, a

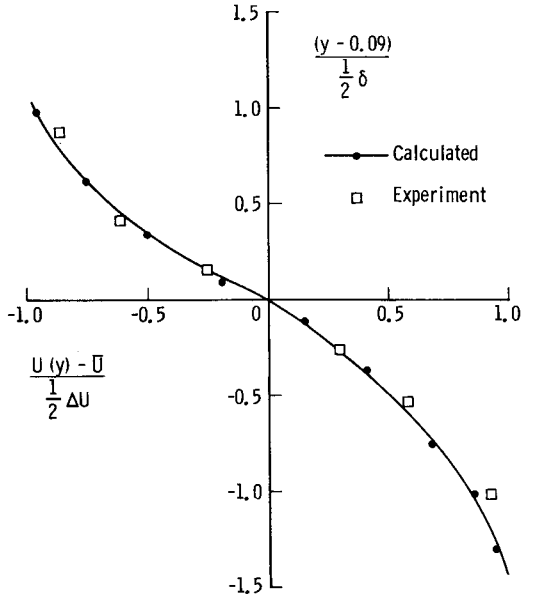

Fig. 11 Comparison of calculated and experimentally measured mean velocity profiles of mode II mixing layer.

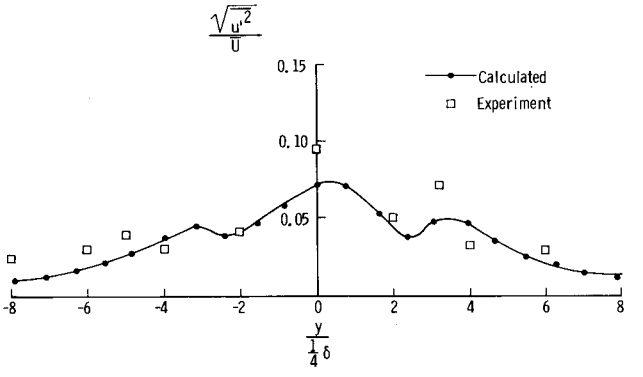

Fig. 12 Comparison of calculated and experimentally measured streamwise velocity fluctuations of mode II mixing layer.

vortex may be stretched and possibly torn apart in the strain fields produced by its neighbors. This behavior was found in Ref. 15. It should be noted, however, that in this case,[15] the high-speed flow is on top, which produces a 180 deg phase shift in the roll-up points. Thus, when the forcing and response frequencies are in phase, vortices are formed at the nodes of the forcing frequency curve and merging is inhibited, while a phase shift of 180 deg is most favorable to coalescence.

To verify this behavior, two cases were run for the mode II mixing layer with phase shifts of 0 and 180 deg. The results are shown in Figs. 14a and 14b. It was found that merging was quite well developed in both instances. Thus, another phenomenon would seem to be at work. Consider once again the situation shown in Fig. 13b. The reasoning given up to this point assumes that no net vertical velocity is induced on any vortex by its neighbors if they are equally spaced. This is not the case in a spatially developing mixing layer. Vortex strengths vary as the structures evolve downstream and the net effect in the present case is to induce an upward velocity on each vortex. This produces a slight upward shift into the low-velocity region and thus their propagation velocity is retarded. The net result is a backward, or upstream, shift in the vortices relative to the forcing waveform, causing a decrease in the effective phase angle. Thus, to achieve the maximum stretching situation, a higher phase angle must be used. To verify this fact, a run was made with a phase angle of 225 deg between the fun-

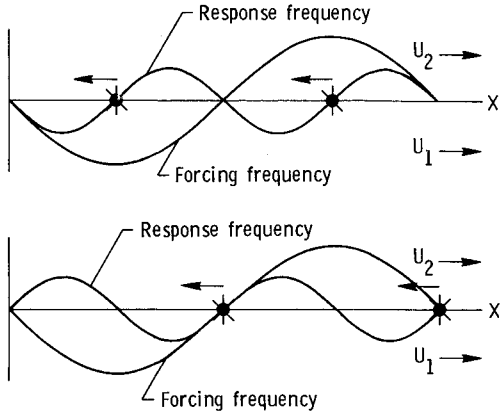

Fig. 13 Effect of phase relationships on vortex evolution patterns.

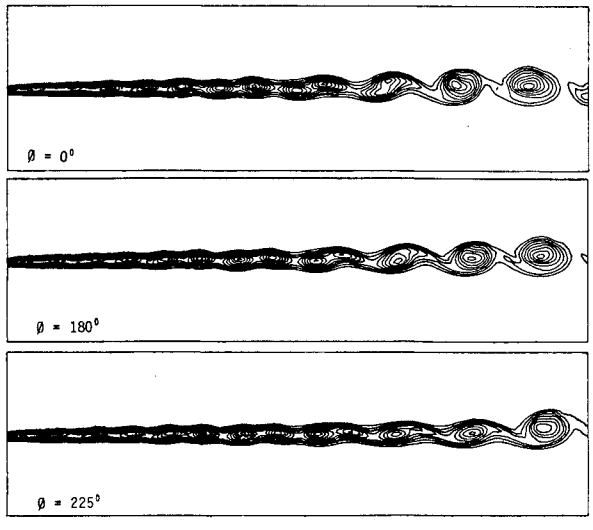

Fig. 14 Effect of phase angle on mixing layer evolution.

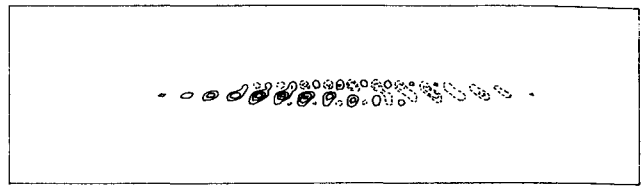

Fig. 15 Contours of $u'v'$ for a mode I mixing layer.

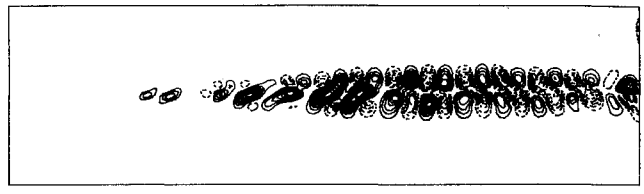

Fig. 16 Contours of $u'v'$ for a mode II mixing layer.

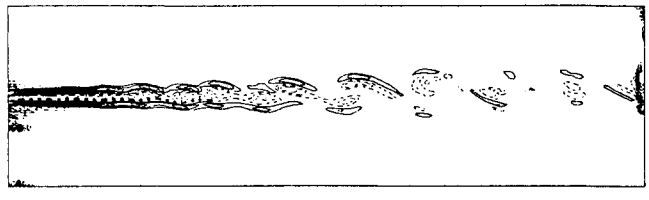

Fig. 17 Contours of viscous terms for a mode II mixing layer.

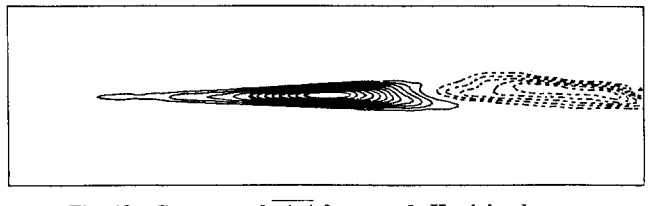

Fig. 18 Contours of $\overline{u'v'}$ for a mode II mixing layer.

damental response frequency and the forcing subharmonic. The results are shown in Fig. 14c. As can be seen, the pairing process is indeed inhibited and the vortex stretching is much more pronounced.

An important point to remember is that it is the spatial accuracy of the present scheme that allows it to model this effect. Any solution technique using periodic boundary conditions cannot account for the difference in induced velocity caused by vortex evolution.

Next, the large-scale contributions to the Reynolds stresses were investigated. Contour lines of instantaneous $u'v'$ values for a mode I mixing layer are shown in Fig. 15. The solid lines are positive, the dashed lines negative. A comparison with Fig. 5 shows that the momentum transport terms are small until roll-up begins and then become very strong as momentum is transferred from the mean flow to the large-scale structure. Note that in this region, the momentum transport is predominantly positive, as it should be for transfer of high-momentum fluid to lower-momentum areas. As the flow evolves downstream, the predominant sign becomes negative, indicating a reversal in the momentum transport direction. Energy begins to be transferred from the large-scale structures back to the mean flow. This is the mechanism that causes the shear layer collapse mentioned earlier.

Figure 16 shows the instantantous $u'v'$ distribution for the mode II mixing layer of Fig. 6. The same comments apply with the additional observation that the very intense positive regions of momentum transport are associated with the pairing process. This indicates that the merging phenomenon is indeed governed largely by inviscid effects. Consideration of the distribution of the viscous terms for a mode II mixing layer will confirm this fact. A plot of these terms for this same mode II configuration is shown in Fig. 17. As can be seen, viscous effects are very pronounced in the initial shear layer regions before roll-up occurs, but are negligible once the dominance of the large scales is established. They seem to be associated primarily with vortex cores and with regions where "braids" of vorticity are being stretched between two structures.

To gain further insight into the interaction processes of the large scale structures with the mean flow, a time average of the $u'v'$, $\overline{u'v'}$, was computed over the mode II flowfield. The results are shown in Fig. 18. The dominance of the positive momentum transport terms (solid lines) in the initial roll-up of the shear layer and its downstream evolution through vortex coalescence is clearly indicated. The intensity of the $\overline{u'v'}$ term in the region corresponding to the initiation of vortex pairing indicates that this process is indeed dominated by momentum transport from the mean flow to the vortical structures. The change to negative contours (dotted lines) after the completion of vortex merging corresponds to the shear layer collapse mentioned earlier. Momentum and energy transfer from the large-scale structures back to the mean flow dominates this region.

Conclusions

The ability of the present computational approach to model accurately the development and interaction of large-scale vortical structures in an evolving mixing layer has been

established by comparison with experimental results. The importance of providing both spatial and temporal resolution of the flowfield in the investigation of such phenomena as phase effects has been demonstrated. Momentum and energy transport from the mean flow to the large-scale vortical structures has been identified as the dominant mechanism of shear layer roll-up and vortex coalescence.

Acknowledgments

This work was supported in part by NASA Cooperative Agreement NCCI-22. The authors would like to thank Prof. C. M. Ho for his cooperation in sharing with us his experimental data and for his insight into the analysis of the results.

References

[1]Hefner, J. N. and Bushnell, D. M., "An Overview of Concepts for Aircraft Drag Reduction," *Special Course on Concepts for Drag Reduction*, AGARD-R-654, June 1977, pp. 1.1-1.30.

[2]Hefner, J. N. and Bushnell, D. M., "Slot Injection for Skin Friction Drag Reduction," *Special Course on Concepts for Drag Reduction*, AGARD-R-654, June 1977, pp. 3.1-3.12.

[3]Howard, F. G., Hefner, J. N., and Srokowski, A. J., "Multiple Slot Skin Friction Reduction," *Journal of Aircraft*, Vol. 12, Sept. 1975, pp. 753-754.

[4]Brown, G. L. and Roshko, A., "On Density Effects and Large Structure in Turbulent Mixing Layers," *Journal of Fluid Mechanics*, Vol. 64, 1974, pp. 775-815.

[5]Dimotakis, P. E. and Brown, G. L., "The Mixing Layer at High Reynolds Number: Large Structure Dynamics and Entrainment," *Journal of Fluid Mechanics*, Vol. 78, 1976, pp. 535-560.

[6]Winant, C. D. and Browand, F. K., "Vortex Pairing: The Mechanism of Turbulent Mixing Layer Growth at Moderate Reynolds Number," *Journal of Fluid Mechanics*, Vol. 63, 1974, pp. 237-255.

[7]Browand, F. K. and Weidman, P. D., "Large Scales in the Developing Mixing Layer," *Journal of Fluid Mechanics*, Vol. 76, 1976, pp. 127-145.

[8]Ho, C. M. and Huang, L. S., "Subharmonics and Vortex Merging in Mixing Layers," *Journal of Fluid Mechanics*, Vol. 119, 1982, pp. 443-473.

[9]Gatski, T. B., Grosch, C. E., and Rose, M. E., "A Numerical Study of the Two-Dimensional Navier-Stokes Equations in Vorticity-Velocity Variables," *Journal of Computational Physics*, Vol. 48, No. 1, Oct. 1982, pp. 1-22.

[10]Gatski, T. B. and Grosch, C. E., "Embedded Cavity Drag in Steady and Unsteady Flows," *AIAA Journal*, Vol. 23, July 1985, pp. 1028-1037.

[11]Acton, E., "The Modeling of Large Eddies in a Two-Dimensional Shear Layer," *Journal of Fluid Mechanics*, Vol. 76, 1976, pp. 561-592.

[12]Kiya, M. and Mikio, A., "Formation of Vortex Streets in Shear Flow," *Applied Scientific Research*, Vol. 34, 1978, pp. 313-339.

[13]Rosenhead, L., "The Formation of Vortices from a Surface of Discontinuity," *Proceedings of the Royal Society of London*, Ser. A., No. 134, 1931, pp. 170-192.

[14]Zalosh, R. G., "A Discrete Vortex Simulation of Finite Amplitude Kelvin-Helmholz Instability," *Proceedings of the Second Computational Dynamics Conference*, Hartford, Conn., June 1975, pp. 205-219.

[15]Riley, J. J. and Metcalfe, R. W., "Direct Numerical Simulation of a Perturbed, Turbulent Mixing Layer," AIAA Paper 80-0274, 1980.

[16]Michalke, A., "On Spatially Growing Disturbances in an Inviscid Shear Layer," *Journal of Fluid Mechanics*, Vol. 23, 1963, pp. 521-544.